Collective dynamics of tunable active chiral particles

Baat, Lotte de

Collective dynamics of tunable active chiral particles

THESIS

submitted in partial fulfillment of the
requirements for the degree of

BACHELOR OF SCIENCE
in
PHYSICS

Author :	Lotte de Baat
Student ID :	s2813599
Supervisor :	Alexandre Morin
Second corrector :	Silke Henkes

Leiden, The Netherlands, June 14, 2024

Collective dynamics of tunable active chiral particles

Lotte de Baat

Huygens-Kamerlingh Onnes Laboratory, Leiden University
P.O. Box 9500, 2300 RA Leiden, The Netherlands

June 14, 2024

Abstract

This thesis investigates the dynamics of tunable active chiral particles, aiming towards the creation of a chiral fluid. The unique aspect of this research is that our individual spinning particles do not have an imposed rotation-orientation distribution, and they are dynamically tunable through combined electrokinetic effects. We analyze both the single-particle behaviour and the collective dynamics over a range of packing densities and concentrations, to identify basic parameters that influence motion and interactions. Our findings demonstrate the effects of packing density and activity in this active particle system, and reveal both fundamental dynamics and intricate phenomena such as cluster formation and spin-spin correlations.

Contents

Version of June 14, 2024– Created June 14, 2024 - 14:44

Chapter 1

Introduction

Chirality is a geometric property of asymmetry observed in various systems in biology and soft matter physics. In active matter, it can give rise to complex behaviours, like the chirality-driven motion of flagella on cells or the formation of chiral patterns in self-propelled particles on a collective level [1], potentially realizing the formation of complex structures with unique properties. Knowing the influence of chirality in such system is necessary for understanding their behaviours and exploiting the potential applications.

The primary goal of this research is to lay the groundwork for creating a chiral fluid, a fluid with an intrinsic handedness and where its constituent particles are chiral themselves. Such chiral fluids are interesting because of their unconventional behaviour, particularly its odd responses, which are not present in typical fluids, such as the emergence of unusual flow patterns, or non-reciprocal viscosity effects.

While the creation of such chiral fluids stays a long-term objective, this research focuses on the study of the individual dynamics towards the collective dynamics of these chiral particles, with the unique property of being able to tune some of the dynamical parameters. This is achieved by exploring the combined effects of Quincke electro-rotation on plastic beads and contact charge electrophoresis on metal beads. As previous studies investigated chiral systems consisting of particles with an imposed rotational distribution, this research uniquely investigates particles with a random and independent rotation. Through a combination of experimental exploration and theoretical analysis, the research attempts to discover some of the collective phenomena.

We will investigate the spin-spin correlation in densely packed systems to understand if and how these particles influence each other while in mo-

tion. Although the creation of a chiral fluid with tuneable parameters remains a future goal, we are making a crucial foundation for future developments in the field.

Version of June 14, 2024– Created June 14, 2024 - 14:44

Chapter 2

Theory

2.1 Chirality

Chirality is a term used for describing a property of asymmetry. More specifically, something is chiral if its mirror image cannot be superposed onto it. Chirality is often referred to in molecules, in that case called 'enantiomers' [2]. Understanding their activity is crucial due to their effects in biological systems.

Next to chirality in molecules, it is an important concept in material science, especially in soft matter, where chiral particles of different sizes can form complex collective structures. Some macroscopic examples of chiral objects are hands or a snail shell, these can be given a handedness:

Figure 2.1: *A snail shell is a macroscopic example of a chiral object, meaning its mirror image cannot be superposed onto it.*

In addition to static geometric chirality, dynamically chiral systems also exhibit a handedness. For example, an object rotating clockwise cannot be superposed onto its counterclockwise rotating mirror image. In the case of a chiral fluid, a collective flow would for example display vortices

with either handedness at one or multiple locations in the system. In the case of a system consisting of many individual dynamically chiral particles, an earlier study showed it is expected to find a collective flow which exhibits chiral behaviour [3].

For a chiral fluid to emerge, the constituent particles should have geometric or dynamic asymmetry, and thereby breaking the system's symmetry under parity (flow does not behave symmetrically with respect to spatial reflections) and temporal inversion (particles would not move back in the same way as they would move forward in time). This behaviour is typically observed in non-equilibrium steady states [4], which are states that remain constant over time but an external force prevents the system from reaching equilibrium.

2.2 Quincke electro-rotation

An insulating particle can start rotating in a conductive solvent under a constant electric field due to the effects of Quincke electro-rotation.

When considering a capacitor with two conductive plates separated by a conductive solvent, applying a voltage across the plates causes charges to accumulate on the plates. A dielectric particle in this system can become polarized when it is exposed to the electric field. This polarization results in a dipole moment that aligns with the direction of the induced electric field within the particle.

The induced dipole in the particle is anti-parallel to the applied electric field, causing surrounding charges to distribute on the particle's surface. As the dipole tends to align with the applied electric field, this could lead to spontaneous symmetry breaking. Any rotational displacement around the axis of rotation produces a steady dipole angle, producing a torque that causes the particle to rotate with a constant velocity in any direction perpendicular to the applied electric field [5]. The magnitude of the torque, and thus velocity of the particle, increases with the strength of the electric field (see section 6.1).

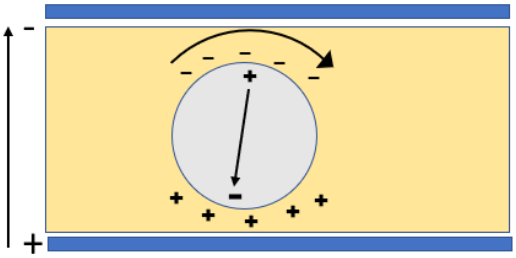

Figure 2.2: *A dielectric sphere in a conductive solvent exposed to an electric field can undergo Quincke electro-rotation. The dielectric particle becomes polarized and any rotational displacement around the axis of rotation produces a steady dipole angle and results in a constant torque.*

2.2.1 Quincke threshold

For relatively low values of the electric field, the insulating bead is stationary; the frictional force experienced by the bead is larger the driving force. Only for high enough values of the electric field, the particle experiences a large enough torque producing rotation. This threshold value for the electric field is called the Quincke threshold [6].

$$E_Q^2 = \frac{2\sigma_s\eta_s\left(\frac{\sigma_p}{\sigma_s}+2\right)^2}{3\epsilon_s^2\left(\frac{\epsilon_p}{\epsilon_s}-\frac{\sigma_p}{\sigma_s}\right)^2} \tag{2.1}$$

This threshold is dependent on the conductivities (σ), the permittivities (ϵ) and the viscosity (η) of the particle (p) and the solvent (s). In the case of an insulating sphere: $\sigma_p = 0$, which reduces the equation as follows:

$$E_Q^2 = \frac{8\sigma_s\eta_s}{3\epsilon_s\epsilon_p} \rightarrow E_Q = \sqrt{\frac{8\sigma_s\eta_s}{3\epsilon_s\epsilon_p}} \tag{2.2}$$

Above the Quincke threshold as shown in equation 2.2, we expect to observe rotation of the particle.

2.3 Contact charge electrophoresis

Consider the same system as the Quincke electro-rotation, where two conductive plates are separated by a conductive solvent. A conductive particle placed in this solvent, exposed to a constant electric field could start

Version of June 14, 2024– Created June 14, 2024 - 14:44

oscillating between the conducting plates, which is called contact charge electrophoresis [7].

During contact between the conductive bead and the electrode, the particle will obtain the charge from the electrode. As now both the electrode and the bead are like-charged, there is a repulsive electrostatic force on the charge:

$$\vec{F}_e = qE_0 \tag{2.3}$$

Where q is the charge acquired by the conductive sphere of radius a due to contact with the electrode and subjected to an electric field E_0 [8]:

$$q = \frac{2}{3}\pi^3 \epsilon_s \epsilon_0 a^2 E_0 \tag{2.4}$$

Where ϵ_s and ϵ_0 are the solvent and vacuum permittivities, respectively. Other forces working on the bead, are the gravitational force and the hydrodynamic drag force [9]:

$$\vec{F}_g = \frac{4}{3}\pi a^3 (\rho_p - \rho_s) g \tag{2.5}$$

$$\vec{F}_d = 6\pi\eta a\vec{v} \tag{2.6}$$

where in equation 2.5 the ρ_p and ρ_s are the densities of the particle and the solvent, respectively, and g is the gravitational acceleration on earth. η in equation 2.6 refers to the viscosity of the solvent and $\vec{v}$ is the velocity of the particle.

The particle can move away from the bottom electrode towards the upper electrode if the (upward) electrostatic repulsive force is larger than the gravitational force. This happens for the following minimum value of the applied electric field, see section 6.6.1:

$$\vec{E}_0 = \sqrt{\frac{2a(\rho_p - \rho_s)g}{\pi^2 \epsilon_s \epsilon_0}} = 0.62\frac{kV}{mm} \tag{2.7}$$

In this research the distance between the electrodes is 3 mm, which would correspond to a lift-off value of 1.86 kV. Note that this threshold value is not dependent on the conductivity of the solvent. This means that the conductive bead always starts lifting off at the same value for the electric field, however the conductivity does determine how quickly the charge will be dissipated.

When the particle has lifted off of the bottom electrode and is immersed in the conductive solvent, the charge will be dissipated on a timescale τ

Version of June 14, 2024– Created June 14, 2024 - 14:44

$= \frac{\epsilon_s}{\sigma_s}$. The more ions in the solution, the higher the conductivity of the solvent and the lower the timescale to dissipate the charge. This could lead to the bead lifting off, without touching the top electrode. If the bead does reach the top, it gets opposite charge causing the electrostatic force to get opposite sign and accelerates towards the bottom electrode, see section 6.2.

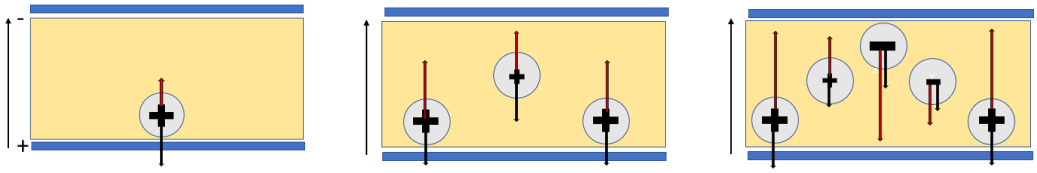

(a) *Conductive bead not lifting off.*

(b) *Conductive bead lifting off, without reaching the top due to dissipation of charges.*

(c) *Conductive bead lifting off and reaching the top where it obtains opposite charge and accelerates down.*

Figure 2.3: *Contact charge electrophoresis can cause a conductive particle placed between conductive plates and immersed in a conductive solvent to start oscillating when exposed to a constant electric field. The height it will reach depends on the balance of the electrostatic force (red arrow) and the gravitational force (black arrow).*

2.4 Conductivity of AOT in hexadecane

In this research, hexadecane with a dissolved salt (dyoctyl sulfosuccinate sodium: AOT) is used as the conductive solvent. The conductivity of the solvent is adjusted by varying the AOT concentration in hexadecane. AOT can form reverse micelles that carry ions, thereby allowing for conductivity of the solvent [10].

A previous study showed that the solvent shows a dependence on solute concentration of the following form [11]:

$$\sigma_s \propto [AOT]^{1.47} \tag{2.8}$$

Where σ_s is the conductivity of the solvent, without exposed to an applied electric field. Combining this result with the Quincke threshold value (see equation 2.2), we get

$$E_Q \propto \sqrt{[AOT]^{1.47}} = [AOT]^{0.735} \tag{2.9}$$

The exact numbers depend on various factors like the amount of water in the AOT.

2.5 Dynamics

In this research, we aim to explore the possibility of generating a fluid composed of dynamically chiral particles with tuneable parameters. These particles are created by glueing a stainless steel bead (1.0 mm in diameter) to a POM bead (1.588 mm in diameter). By combining the effects of Quincke electro-rotation on the POM bead and contact charge electrophoresis on the metal bead, we investigate some tuneable dynamics, including the radius of gyration and the angular velocity.

2.5.1 Mean Squared Displacement

We do not only study the spinning characteristics but also the diffusive behaviour of these particles, both individually and with neighbouring particles.

To understand the diffusive properties, we investigate the mean squared displacement (MSD) of the particles, which measures the deviation of a particle's position from its initial position, over time:

$$\mathrm{MSD}(\Delta t) = \left\langle [x(t+\Delta t) - x(t)]^2 \right\rangle_t \tag{2.10}$$

The behaviour of the MSD classifies different types of a particle's motion. If a particle is spatially confined, the MSD flattens after an initial increase. For particles having directed motion, the MSD grows exponentially. For random diffusion, the MSD increases linearly over time [12]. In the last case, the slope of the MSD is related to the diffusion coefficient, which depends on the number of spatial dimensions. The MSD for n-dimensional Brownian motion is given by:

$$\mathrm{MSD}(t) = 2nDt \tag{2.11}$$

Where in equation 2.11, n is the number of dimensions, D is the diffusion coefficient and t is time.

2.5.2 Spin-spin correlation

We also want to understand if particles tend to have any preference for spin orientation, based on the spin orientation of particles within a certain

Version of June 14, 2024– Created June 14, 2024 - 14:44

radius around that particle. Therefore we look at the spin-spin correlation, which is defined as follows:

$$C_{ss} = \langle C_{ss}(\Delta r, t) \rangle = \langle \langle S(r_o, t) \cdot S(r_o + \Delta r, t) \rangle \rangle_{r_o, t} \tag{2.12}$$

In equation 2.12, the spin values can be either +1 or -1, which represent their spin orientation. To calculate the spin-spin correlation C_{ss}, we consider the spin of a particle $S(r_o, t)$ and multiply it by the spin of another particle in the neighbourhood at the same time $S(r_o + \Delta r, t)$, so that particles with the same spin get a value of +1 and opposite-spin particles get a spin correlation value of -1.

For each particle, we perform this calculation with the neighbouring particles within a certain radius. The resulting values are averaged over all particle positions and times to obtain the overall spin-spin correlation of the system.

2.6 Collective motion of spinning particles

In the case where spinning particles self rotate ($\omega \neq 0$) but not self propel ($v_0 = 0$), the individual particles do not show any translational motion. However when colliding, the friction between the spinners can transform rotational motion into translational motion. This induces time reversal symmetry breaking of translational degrees of freedom. So if the velocity and momenta after the collision would be reversed, the particles would not move back in the same way they moved forward during the collision [13].

An earlier study showed that the collective dynamics of driven spinning particles are governed by two main parameters: packing density (ϕ) and angular velocity (ω_0) [14]. Bringing rotating particles together would give three expected categories; for low packing density the spinners are fixed in place and because there are not many collisions there is no translational motion coupled to rotation. In this regime the drag force dominates. For increased packing density, a fluid phase is observed. As more collisions will happen, there is more transfer from rotational to translational motion leading to collective flows. For the highest packing density they observed rotating crystals.

This study also showed that when two opposite asymmetric spinners collide head-on, the tangential velocities of their 'arms' align in the same direction, causing them to move together briefly before moving apart. Conversely, when two spinners with the same spin orientation collide,

their 'arms' have tangential velocities in opposite directions, causing them to stick together at the point of contact. This results in transfer of angular momentum, causing them to possibly rotate together momentarily before moving apart [14], see section 6.4.

Version of June 14, 2024– Created June 14, 2024 - 14:44

Chapter 3

Methods

3.1 Experimental set up

The particles used in this research consist of a stainless steel spherical bead (1.0 mm in diameter), glued to a plastic (polyoxymethylene; POM) spherical bead (1.588 mm in diameter). The composite particles are confined in a circular frame, covered with a metallic part on one side, placed at the bottom of the system to repel the metal beads from the inner edges, ensuring that the particles move freely in the center of the system. This frame must be large enough to provide an appropriate area-to-edge ratio, allowing most particles to move freely in the center.

The used conductive solvent consists of hexadecane with a dissolved salt (dyoctyl sulfosuccinate sodium: AOT). The conductivity of this solvent can be adjusted by varying the AOT concentration, which is essential for investigating the motion of the particles at different conductivity levels. The solvent is brought into the system through tubes passing through the outer square frame. The distance between the glass plates is 3 mm, providing a regime in which the metal bead bounces, but particles can hardly exist on top each other. Therefore the particles are only observed in two dimensions from the top.

To initiate the Quincke electro-rotation on the plastic bead and contact charge electrophoresis on the metal bead, a DC voltage is applied to create an electric field between the two conducting glass plate. The function generator operates within a range of 0 to 5 volts, and an amplifier is used to amplify this by a factor of 1000 (gain). To perform reliable experiments it is crucial to use a well-cleaned device, including all components.

3.2 Procedure outline

To investigate the motion of the particles at different packing densities, we first study the motion of a single particle. These measurements are performed in a system at concentrations of 20mM, 60mM and 100mM (mM = millimolar) AOT in hexadecane. We perform independent measurements by switching the generator on and off between each trial. The single particle experiences no interaction with other particles or the systems' edges, so it is only being influenced by the friction of the solvent, allowing it to rotate freely.

Next, we investigate the motion of particles at packing densities Φ = 10% and Φ = 40%. We try to determine how the motions of these denser systems differ from the motion of a single spinning particle, see section 6.6.2.

Interestingly, activating a single spinner is more challenging than activating a denser system under the same circumstances. In a denser system, the movement of a few particles activates neighbouring particles, requiring only a little initial push. Conversely, a single particle often requires a tap on the upper plate to initiate its motion. To collect data on the particle's motion, we record the active system with a top-view camera, capturing a two-dimensional view.

Recordings are stored as many successive frames. We use a code that detects the particles in all those frames. Afterwards we find their trajectories over time. To have reliable data, we require a high enough frame rate, which was determined to be 150 frames per second in this research.

We are only tracking the motion of the POM beads and comparing their motion in different environments.

3.3 Extracting dynamics

To find the basic dynamical properties of a single and multiple particle system, we use a code that finds the percentage of stationary particles, mean radius of gyration, mean angular velocity, diffusion coefficient and spin correlation.

3.3.1 Percentage stationary particles

To determine the percentage of stationary particles in denser systems, we look at the number of particles that have a radius of gyration smaller than

Version of June 14, 2024– Created June 14, 2024 - 14:44

7 pixels. By plotting the distribution of the radii of gyration for the multi-particle system, we observe a clear distinction between the mean radius of gyration of moving particles and (nearly) stationary particles. For a single particle, no motion was recorded with a radius of gyration smaller than 10 pixels. Making this distinction is important because of the dependency of the radius of gyration in the calculation for the angular velocity.

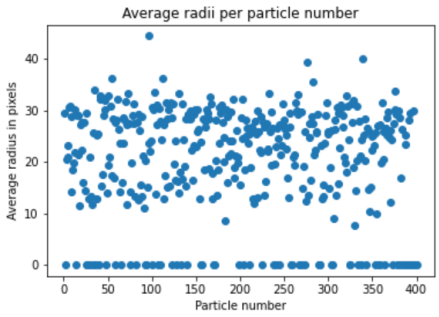

Figure 3.1: *Example distribution of radii of gyration for a multi-particle system. A clear distinction is observed between the measured radii of gyration of moving particles and (nearly) stationary particles. A particle is considered stationary for a radius smaller than 7 pixels.*

3.3.2 Radius of gyration

We determine the mean radius of gyration of a particle by iteratively analyzing 6 consecutive positions. We fit a circle to this subset to determine the radius of this best-fitted circle. Then we shift to the next frame and repeat this process. This is iterated for all possible subsets, to finally determine the mean value for the particle's radius of gyration.

3.3.3 Angular velocity

To calculate the mean angular velocity of a spinning particle, we look at the distance travelled between two consecutive frames, the radius of gyration that corresponds with those points and the time between the two positions. Then we apply the following formula:

$$\omega = \frac{s}{rt} \tag{3.1}$$

where in equation 3.1 s is the distance travelled between two consecutive points, r is the corresponding radius of gyration and t is the time

between two frames. In the denser system, the mean angular velocity is only taken over moving particles, so particles with a radius of gyration of less than 7 pixels are not examined.

3.3.4 Mean squared displacement

To understand the diffusive behaviour of the particles individually and in densely packed systems, we look at the mean squared displacement (MSD). To compute the MSD for a single particle, we take the square of the difference between its current position and its initial position at each time step and plot these outcomes against time. For a multiple particle system, the MSD is determined by taking the square of the differences between the current and initial positions for each particle and each time step, and then compute the mean of the squared differences for each time step over all particles.

To calculate the diffusion coefficient of moving particles we need to look at the slope of the MSD. In this research, we observe our system in two dimensions, so according to equation 2.11 the slope of our MSD is 4D.

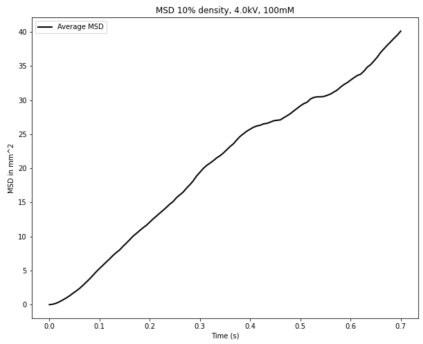

Figure 3.2: *The MSD for a multiple particle system is calculated by taking the square of the differences between the current and initial positions for each particle and each time step, and then compute the mean of the squared differences for each time step over all particles. The MSD gives insight on the diffusive properties of the system.*

3.3.5 Spin distribution

To determine the spin of a particle in the system, we analyze the trajectory of the particle over 3 successive frames. Let r_{t-1}, r_t and r_{t+1} be the positions of a particle at time $t-1$, t and $t+1$. From these positions, we

find two displacement vectors: $\vec{A}$ is the displacement of the particle from r_{t-1} to r_t and $\vec{B}$ is the displacement of the particle from r_t to r_{t+1}. Then we take the cross product of the vectors $C = \vec{A} \times \vec{B}$. If $C < 0$, the particle is rotating clockwise and if $C > 0$, the particle is rotating counterclockwise.

To determine the overall spin distribution of the system, we sum over the spin values for each particle at all times in the system based on this method. This is a cumulative distribution and covers the rotational behaviour of the entire multi-particle system. Next to the overall spin distribution, we find the most likely spin value for each particle by determining the most frequent orientation across all frames. Eventually we determine if the distribution is random or not, by performing a chi-squared analysis. This is done by comparing the observed distribution of spin values with the expected distribution of spin values, assuming a random distribution:

$$\chi^2 = \sum_i \frac{(O_i - E_i)^2}{E_i} \tag{3.2}$$

where in equation 3.2 the O_i is the observed count for category i and E_i is the expected count for category i, assuming randomness. In this research, we have the two categories of clockwise spin and counterclockwise spin. Based on the χ^2 analysis we determine the corresponding p-value, which measures the strength of evidence against the null hypothesis. A small p-value represents strong evidence against the null hypothesis, indicating that the observed distribution significantly differs from randomness, while a higher p-value suggests a random distribution.

In order to calculate the p-value, the number of degrees of freedom in the system need to be known, as well as the χ^2 value. The number of degrees of freedom can be calculated using $df = k - 1$ where k is the number of categories, which in this research, $k = 2$, because the particle can either spin clockwise or counterclockwise, resulting in one degree of freedom.

The p-value is found with the 'chisquare' function in Python, which analyzes the cumulative distribution function of the χ^2 distribution for the given χ^2 and the number of degrees of freedom. The p-value then represents the probability that a χ^2 value as extreme or more extreme than the observed value could be obtained.

If the p-value is lower than 0.05, it means that there is a significant difference between the observed distribution and the expected distribution assuming the null hypothesis of having a random distribution. A low p-value would mean a small chance of obtaining a higher χ^2 value, therefore allowing to reject the null hypothesis. That suggests that the observed val-

ues are significantly different from the expected values.

3.3.6 Spin-spin correlation

We want to understand if a particle has any preference for spin orientation, based on the spin orientation of the particles in a certain radius around that particle. For this we find the spin-spin correlation as described in equation 2.12, where we look at the spin orientation of a particle at a certain time $S(r_o, t)$ and multiply it by the spin of particles within a certain radius $S(r_o + \Delta r, t)$ so that particles with the same spin get a C_{ss} value of +1 and opposite spins get a C_{ss} value of -1. We perform this calculation for each particle with the neighbouring particles and the results are averaged over all particle positions and time to obtain the overall spin-spin correlation of the system.

Chapter 4

Results and analysis

In this chapter we present the results of the dynamical properties of the single particle and multiple particle system. We will analyse and explain the behaviour of these systems and compare if the behaviour for more densely packed systems is consistent with the single particle results, or differ significantly. Additionally we will share the results on the spin-spin correlation in the more densely packed systems, to observe if particles are influenced by the spin orientation from neighbouring particles.

4.1 Regime of interest

The system, composed of spinning particles made of a POM bead attached to a metal bead in a conductive solvent, had many parameters to investigate. However, the measurements were only performed in the regime of interest, meaning the voltages between which the particles start spinning (lowest voltage) and reach the top electrode (highest voltage). These regimes are dependent on the conductivity of the solvent.

For low conductivity, we observed a relatively low required voltage to initiate the spinning motion. This is due to a low Quincke threshold: $E_Q \propto \sqrt{\sigma_s}$. Additionally, the threshold voltage for the metal bead to reach the top electrode was also relatively low, as the charges on the metal bead dissipate slowly on a timescale: $\tau \propto \frac{1}{\sigma_s}$. Therefore, a low conductivity corresponds to a low voltage regime.

Conversely, for a high conductivity, the spinning motion started at a higher voltage due to a high Quincke threshold. Additionally a higher voltage needs to be applied for the metal bead to reach the top electrode, as the charges quickly dissipate. Consequently, a high conductivity corre-

sponds to a high voltage regime.

4.2 Single particle

We will begin by analyzing the dynamics of a single particle in varying AOT concentrations and applied voltages. The goal is to identify the conditions that return the most tuneable properties of the spinning particle. This will be used to to multiply these particles and place them in the same environment, to be used as building blocks for the multi-particle system.

An example trajectory of such a single spinning particle is presented in figure 4.1, where the plotted positions are the centers of the POM bead. From these positions we calculate the spin orientation, radius of gyration, angular velocity and diffusion coefficient.

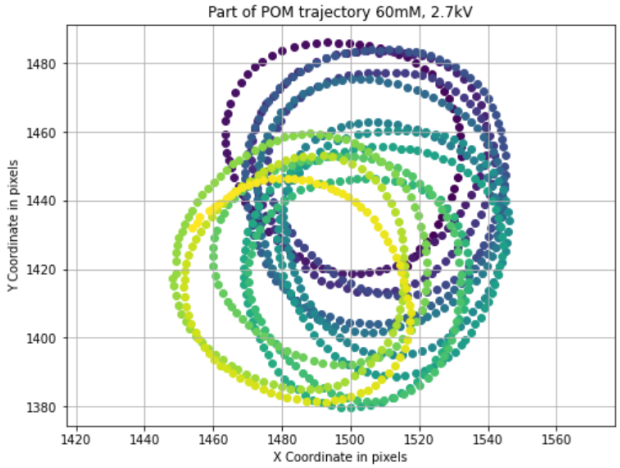

Figure 4.1: *Part of POM trajectory at 60mM, 2.7kV. From the positions we deduce the dynamics.*

4.2.1 Spin distribution

One of the unique properties of our chiral particles is that we expect them to display a random spin distribution. From the Quincke threshold onwards, the POM bead becomes polarized and begins to rotate in a random direction perpendicular to the applied electric field. As the POM bead is attached to the metal bead, the POM bead rotates around the metal bead with an expected equal probability of spinning clockwise or counterclockwise. Here we investigated whether a single particle indeed spins with

a random orientation or if there is a significant preference for a certain direction.

We repeated the experiment with a single spinning particle in the system 218 times, determining the spinning orientation for each measurement. Before every new measurement, we turned off the voltage to make sure that the particle was stationary. The voltage was then increased to start the particle's spinning motion. This was done so that each measurement was independent and not influenced by any motion from the previous measurement.

We found in 115 cases (52.75%) for the experiment a clockwise spin orientation of the spinning particle and in 103 cases (47.25%) a counterclockwise spin orientation of the spinning particle, as presented in figure 4.2:

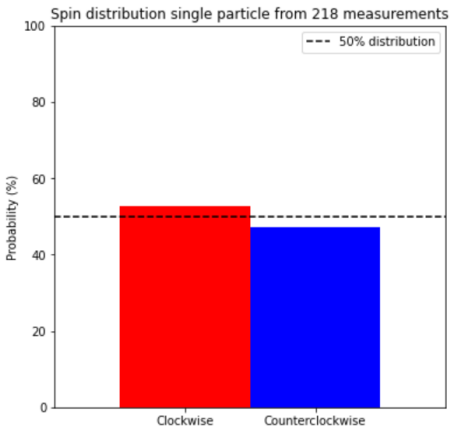

Figure 4.2: *Overall spin distribution of a single spinning particle in a conductive solvent, from 218 measurements. Result is the sum of total observed clockwise spins (red) vs total observed counterclockwise spins (blue). The black dotted line indicates 50%.*

To determine whether this distribution of a single particle is random or if there is a preference for a particular spin orientation, we performed a χ^2 test.

In a perfect random scenario, the expected number of finding both clockwise and counterclockwise spins would be $\frac{218}{2} = 109$. Using equation 3.2, the χ^2 value is calculated to be $\frac{(115-109)^2}{109} + \frac{(103-109)^2}{109} = 0.66$.

To find the p-value, Python's 'chisquare' function evaluates the cumulative distribution function of the χ^2 distribution, given the calculated χ^2 and the degrees of freedom. We find a p-value of 0.42, which is greater than the threshold of 0.05, so we cannot reject the null hypothesis of hav-

ing a random distribution. Therefore, we conclude that the spin distribution is likely random, with no significant preference for a specific spin orientation.

4.2.2 Radius of gyration & angular velocity

We investigate the mean radius of gyration and angular velocity for a single spinning particle over 3 different concentration (20 mM, 60 mM and 100 mM) and various voltages within the regimes of interest. We aim to determine the conditions that give the most tuneable radii of gyration and angular velocities to identify the clearest dependency on voltage to find the optimal conditions for controlling these properties.

The experiments were performed using the same particle and experimental setup for every measurement, in which the only changing variable was the AOT concentration. The results are shown in figure 4.3:

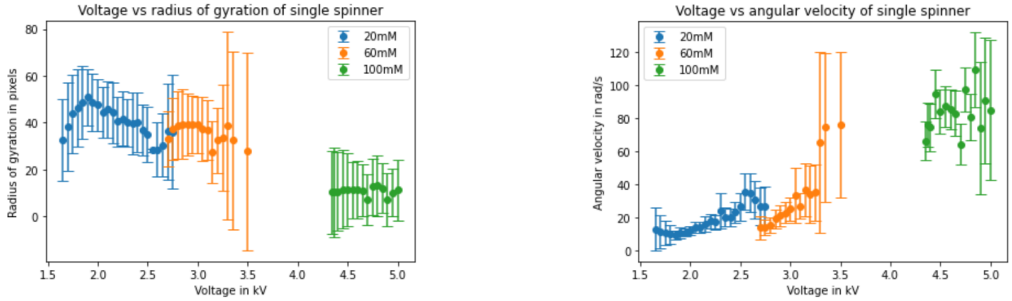

Figure 4.3: *Radii of gyration and angular velocity for a single particle over various voltages in AOT concentrations 20 mM, 60 mM, and 100 mM.*

The initial observation is that each concentration shows its corresponding regime of interest, as discussed in the section 4.1. A higher conductivity of the solvent requires a higher voltage to initiate the motion of the particle because the Quincke threshold is higher for more conductive solvents, see equation 2.9, which states that $E_Q \propto \sqrt{[AOT]^{1.47}}$.

Additionally, we observe that lower concentrations of the solvent generally correspond to larger radii of gyration and smaller angular velocities. This phenomena can be explained by the combined effect of contact charge electrophoresis on the metal bead and Quincke electro-rotation on the POM bead. For the 20 mM and 60 mM concentration, the POM bead clearly spins around the metal bead, dragging the metal bead in circles. The decreased radii of gyration observed at 100 mM can be ascribed to the bouncing of the metal bead and high angular velocities of the POM bead

resulting in the particle to turn around its center of mass instead of the POM bead turning around the metal bead, resulting in a smaller radius of gyration. To give insight in the precise dynamics causing this behaviour, we need to do more research on the bouncing height and displacement of the metal bead.

We observe that there is the clearest dependency between the radius of gyration, angular velocity and voltage for the 20 mM measurements. For this we see an increase in radius of gyration for increasing voltage and decrease in angular velocity (reaches their extremes at 1.90 kV). In this regime, the angular velocity is linearly dependent on the radius: $\omega \propto -Rgyr$. Between 1.65 kV and 1.90 kV the metal bead does not bounce yet, though the POM bead experiences increased torque causing it to drag the metal bead around, so that the metal bead also moves in circles. We will later analyze the transition for the initialization of the bouncing by analyzing the measured angular velocity around these voltages.

Between 1.90 kV and 2.55 kV for the 20 mM measurements, the angular velocity increases and the metal bead starts bouncing. This causes the POM bead to solely spin around the metal bead, without dragging the metal bead. From 2.55 kV onwards we see a linear increase in radius of gyration again and a decrease in angular velocity. Understanding this behaviour requires further research.

For the higher concentrations, the clarity of the dependencies between the applied voltage and radius of gyration seem to diminish. This is due to more noise in the system, causing less controllable behaviour.

In the regime of interest of the 20mM, we expect to find a transition from a non-bouncing regime of the metal bead to a bouncing regime. Therefore we analyzed this transition by plotting the measured angular velocities of the POM bead for every frame number over a range of voltages. A change in angular velocity represents the start of bouncing, and thereby we can identify the transition point:

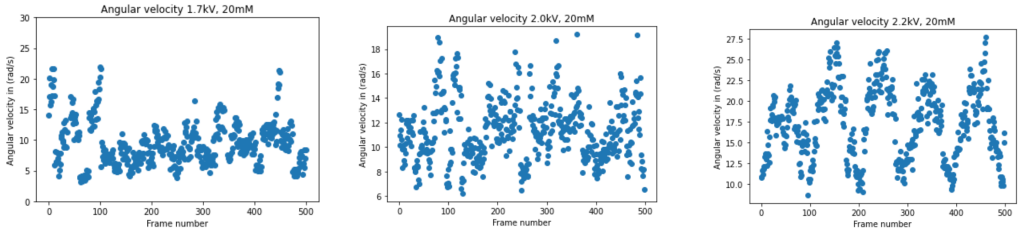

Figure 4.4: *Transition from a mostly constant angular velocity (no bouncing regime, 1.7 kV) to variation in angular velocity (bouncing regime 2.2 kV) The threshold value is roughly 2.0 kV, here the bead starts bouncing.*

In this research, we found that the electric field required to make the bead lift off is approximately 2.0 kV. From theory we expected to find a threshold value of 1.86 kV. This slight increase in field might be due to small accuracy errors in the calculation or materials. This threshold value is not dependent on the conductivity of the solvent, however the conductivity does determine how quickly the charge will be dissipated.

4.2.3 Mean squared displacement

To obtain the mean squared displacement of a single particle over time we calculate the square of the difference between the current position and the initial position at each time step and plot these against time.

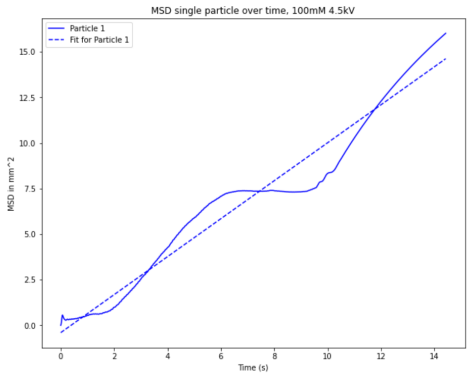

Figure 4.5: *Example of measured MSD of a single particle in 100 mM, 4.5 kV. A line of best fit is plotted through the data to calculate the slope to find the corresponding diffusion coefficient.*

As shown in figure 4.5, we plot the MSD with the line of best fit and calculate the slope of this line. The slope of the line is proportional to the diffusion coefficient of the particle. In our system, we observe a two-dimensional top view, so according to equation 2.11, the slope of the calculated MSD is 4D, where D is the diffusion coefficient.

The results of the obtained values for the diffusion coefficient are plotted in figure 4.6:

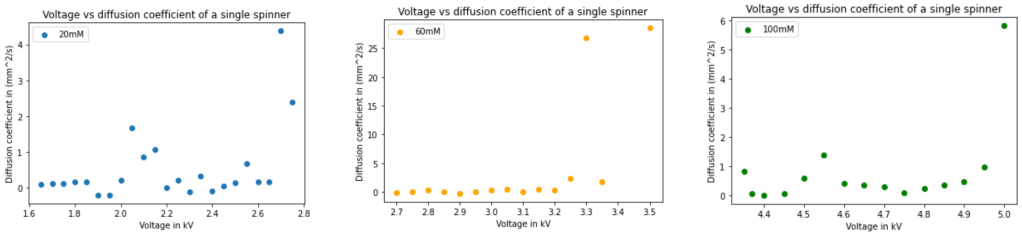

Figure 4.6: *Diffusion coefficients for a single particle in 20 mM, 60 mM and 100 mM in each regime of interest, respectively.*

From these results, we notice several leading observations. For the 20 mM concentration, at the lowest voltages, the diffusion coefficient is low. However, between 2.0 kV and 2.2 kV there is an increase, which might be explained by the fact that the metal bead starts bouncing, which induces some diffusive behaviour as a result of the unsteady nature of this transition point. At the higher voltages, the bouncing becomes more stable as angular velocity increases, resulting in more consistent spinning and reduced diffusive behaviour.

At the highest measured voltages, just before the metal bead reaches the top electrode, the diffusion coefficient increases to a maximum value which is observed for all concentrations. At this point the POM bead drags the metal bead around, reducing its effectiveness as an anchor and contributing to the diffusive behaviour.

Even though the shape of the 100 mM concentration is very similar to the 20 mM concentration, it probably does not have the same nature. As the increase in the 20 mM is most likely caused by the initialization of the bouncing metal bead, the slight increase in diffusive behaviour between 4.5 kV and 4.6 kV is likely due to noise in the system.

4.3 Multiple particle system

Having examined the behaviour of a single spinning particle across various concentrations, the next step is to determine whether the behaviour is influenced or remains unaffected by neighbouring spinning particles.

The regimes of interest for the multiple particle system might differ slightly from the single particle system. This could have various reasons, for example that it is challenging to activate a single particle, which requires a small external force, while in a denser system the movement of a few particles activates the neighbouring particles, requiring only a little initial push. Or, conversely, that the densely packed system has a high

percentage of stationary particles, restricting other particles movements.

Finally we will examine if the particles influence each others spin orientation, by finding the spin-spin correlation for neighbouring particles in these systems.

4.3.1 Radius of gyration and angular velocity

We investigate the radius of gyration and angular velocity for the 10% and 40% packing density systems in the 20 mM and 100 mM concentrations in their respective regimes of interest to see if this behaviour is similar or different to the single particle measurements. We will find how this movement might be influenced due to the effect of neighbouring particles. The 60 mM concentrations measurements had similar observations as the 20 mM measurements, but due to different behaviours in the system we observed relatively unclear correlation, these results can be found in section 6.7.

The experiments were performed using the same experimental setup, in which we only changed the number of particles and the AOT concentration. The results for the radius of gyration and angular velocity as a dependency on voltage for 10% and 40% packing density for the 20 mM concentration are presented:

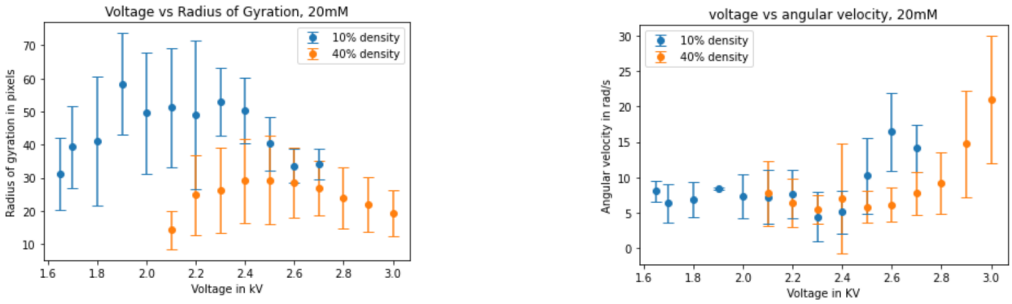

Figure 4.7: *Radius of gyration and angular velocity for the 10% and 40% packing density systems at 20 mM.*

In figure 4.7 we observe that for the 20 mM system, where we have a transition from a non-bouncing regime to a bouncing regime, there is an increase in angular velocity from approximately 2.4 kV onwards, for both packing fractions. Conversely, we see that from this voltage onwards, the radius of gyration decreases, according to what we expected from equation 3.1. We also saw this behaviour for the single spinner, however, this transition was from a lower voltage onwards.

For the single spinner, we observed radii of gyration between 28 and 51 pixels. For the 10% packing density this is between, 31 and 58 pixels which is a similar regime. This is because in this density, particles have enough space to spin on themselves. For the 40% packing density the observed radii of gyration is between 14 and 30 pixels, which is significantly lower, due to restricted space to move.

We also find the results for the radius of gyration and angular velocity as a dependency on voltage for 10% and 40% packing fraction for the 100mM concentration:

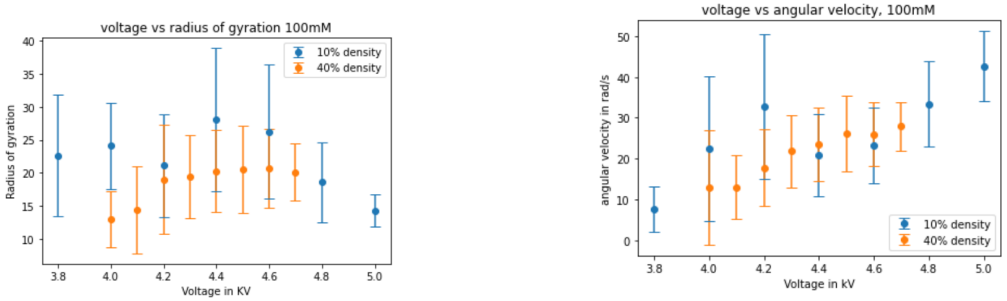

Figure 4.8: *Radius of gyration and angular velocity for the 10% and 40% packing fraction systems at 100mM.*

For the 100 mM we see an immediate increase in angular velocity from the lowest voltage onwards which we did not observe for the 20 mM concentration. The increase in radius of gyration followed by a plateau (40%) and decrease (10%) is similar behaviour as for the 20 mM concentration. At this concentration, there is significantly more diffusive behaviour and with more moving particles than at the previous concentration (we will analyze this in the next sections). The high density of the system restricts the motion of the particles; we do not observe an initial decrease in angular velocity as seen in the lower concentrations because particles diffuse through the system, resulting in an effective increasing angular velocity for increasing voltage.

For the single spinner in 100 mM, we observed radii of gyration between 7 and 13 pixels. For the 10% packing density this is between, 14 and 28 pixels and for the 40% packing density the observed radii of gyration is between 12 and 21 pixels which are both significantly higher than the single particle. We observe these high radii of gyration in 100mM because in the single particle system the particle spins around its center of mass, but in the higher density system the particles experience more collisions, disturbing their spinning motion on the spot, changing trajectories and resulting in a larger effective radius of gyration.

We observe that the radius of gyration for the 40% packing density is generally smaller than that for the 10% packing density across all voltages. This can be attributed to the high density of the system, where particles are constrained in space by their neighbours, preventing them from performing full circular motions. Next to that, the 40% packing density system mostly results in a lower angular velocity compared to the 10% packing density system at the highest voltages. This is because of the increased frequency of collisions in the 40% packing density system, causing more stationary time during collisions and thereby reducing the effective angular velocity. This also explains that angular velocities for the higher densities are lower than for a single particle.

It is interesting to see that the higher the packing density, the clearer the dependencies for the 100 mM concentration. We see a linear increase in the angular velocity for 100 mM, 40% packing density, while for the single particle there is no clear relationship between the radius of gyration and angular velocity at this concentration. In the 40% packing density system, each particle's movement is restricted by its closely packed neighbours, restricting their ability to make full circular motions. As a result, a particle cannot maintain a significantly different radius of gyration from its neighbours and is influenced to move cohesively. So particles will adopt a similar behaviour of the surrounding, resulting in a clear dependency on the applied voltage.

A general observation in figures 4.7 and 4.8 is that for every concentration the 40% density measurements start at a higher voltage compared to the 10% density because the motion was already observed for lower voltages at 10% density. This is because in higher packing density systems we found that there was a lot of cluster formation, causing a high percentage of stationary particles, preventing other particles to move.

4.3.2 Cluster formation & diffusion coefficient

An important factor that should be taken into account for the measurements on the 10% and 40% packing density systems, is that when we apply a relatively low voltage, not all particles are activated to move but tend to form stationary clusters. We have a coexistence of clusters and moving particles.

This is an important note because if we want to lay the basis for the potential chiral fluid with tunable parameters, we want (almost) all particles to move. However, we have observed that in many settings, not all particles are moving in the regime of interest. This restricts us in finding

the ideal environment.

In figure 4.9 the images of a 10% packing fraction system are shown in the case where there are a lot of clusters (20 mM, 1.7kV) but these clusters disappear when a higher voltage is applied (20 mM, 2.7 kV):

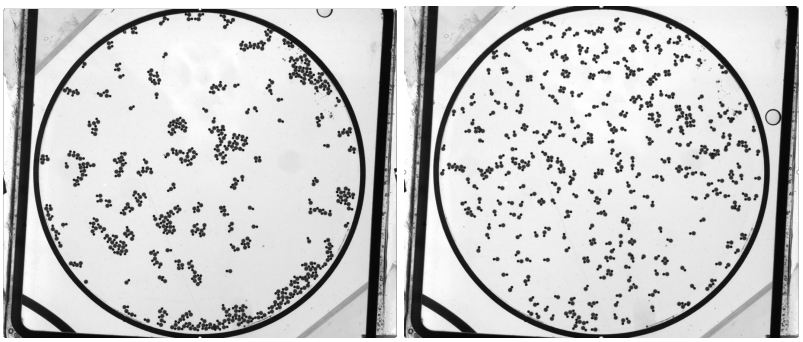

Figure 4.9: *10% packing density 20 mM: stationary cluster formation for lower voltages (1.7 kV) which dissolve for higher voltages (2.7 kV).*

The same happens for a 40% packing density system as shown in figure 4.10 where there are a lot of clusters (100 mM, 4.2kV) but these clusters disappear when a higher voltage is applied (100 mM, 5.0 kV):

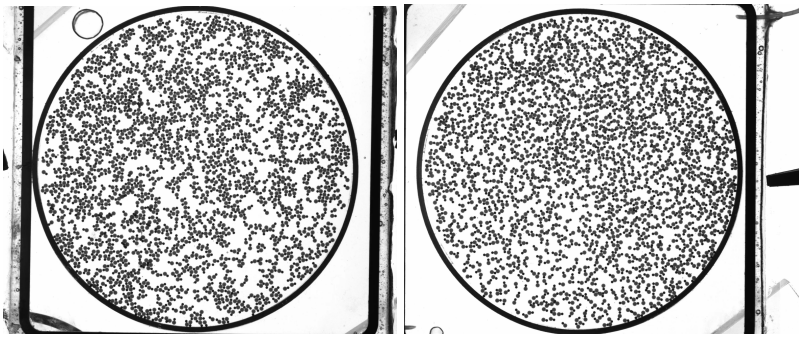

Figure 4.10: *40% packing density 100 mM: stationary cluster formation for lower voltages (4.2 kV) which dissolve for higher voltages (5.0kV)*

It is interesting to analyze the influence of stationary particles on the diffusive properties. We will compare the percentage stationary particles with the diffusion coefficient. Note that the diffusion coefficient will be calculated only for moving particles and we will compare it to the previously calculated diffusion coefficient for the single particle.

We examined the percentage of stationary particles for the 10% and 40% packing densities at 20 mM concentration and compare the behaviour

of the percentage of stationary particles with the diffusion coefficient as shown in figure 4.11:

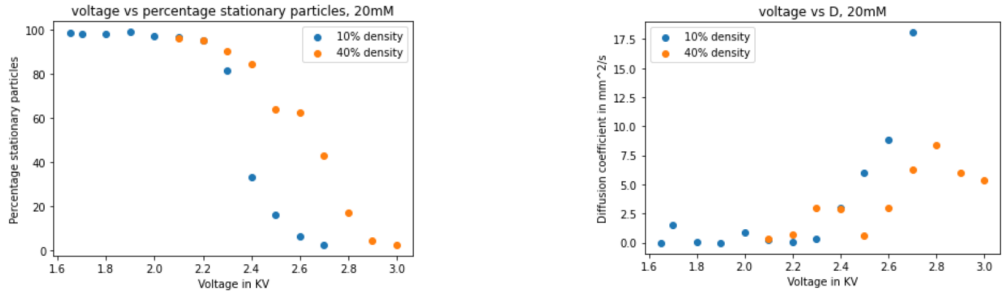

Figure 4.11: *Percentage of stationary particles and diffusion coefficient against applied voltage for 10% and 40% packing density in 20 mM.*

In the 20 mM concentration, we observe a high percentage of stationary particles at lower voltages, which corresponds to a low diffusion coefficient for moving particles. The few particles that do move often stay in place. From 2.3 kV onwards, a transition happens in the number of stationary particles; more particles start to move. In the 10% packing density system we see a clear increase in the diffusion coefficient starting from this voltage; as more particles start moving, the diffusion per particle increases.

This increase in diffusion coefficient starts from a lower voltage than that required for a single particle in this concentration and the diffusion is much higher for increasing voltages compared to the single particle. This difference is due to the interactions between particles: in a gas-like state (10% density), where particles spin on themselves, exert hydrodynamic interactions and collide with each other, causing a significant amount of diffusive motion. The relation between the percentage of stationary particles and diffusion coefficient for the 20 mM 10% fraction is $stationary \propto -\sqrt{D}$. For the 40% this relation does not hold anymore.

For the 40% packing density we also see an increase in diffusion coefficient for increasing voltage, but less pronounced. This is because the particles do not have the space to freely move but are restricted in space by the neighbouring particles. Therefore the particles can not solely spin on themselves and exert hydrodynamic interactions, but most of the diffusive behaviour is caused by the collisions between particles.

The results for the percentage of stationary particles and diffusion coefficient for the 10% and 40% packing densities for the 100 mM concentration are shown in figure 4.12:

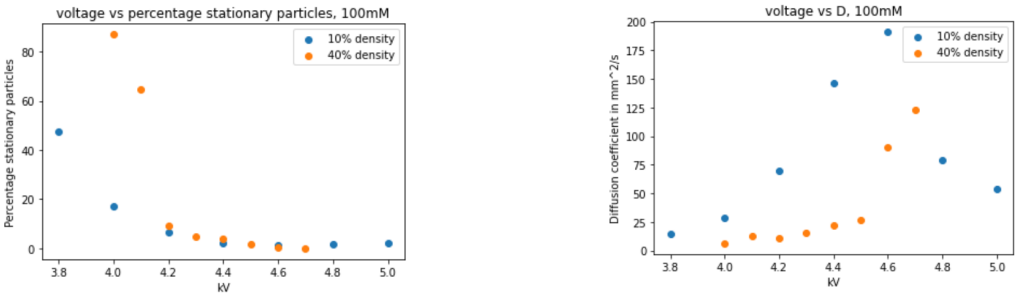

Figure 4.12: *Percentage of stationary particles and diffusion coefficient against applied voltage for 10% and 40% packing fraction in 100 mM.*

For the 100 mM measurement, we observe an exponential decrease in percentage of stationary particles for increasing voltages. Note that the diffusion coefficient values are between 0 and 200 mm^2/s which is significantly higher that at 20 mM where this was between 0 and 18 mm^2/s. This is because the increased angular velocity causes even small collisions to have a powerful impact on neighbouring particles, leading to high impact collisions. In the 10% packing density system, there is an increase in the diffusion coefficient with increasing voltage up to 4.6 kV. However, above 4.6 kV, the diffusion coefficient decreases again in the 10% packing density system. From this point, we also see a decrease in radius of gyration, due to the particle turning around its center of mass instead of the POM bead turning around the metal bead, as observed for the single particle. This fast spinning motion creates hydrodynamic interactions with neighbouring particles, causing them to spin independently in place, reducing the diffusive behaviour.

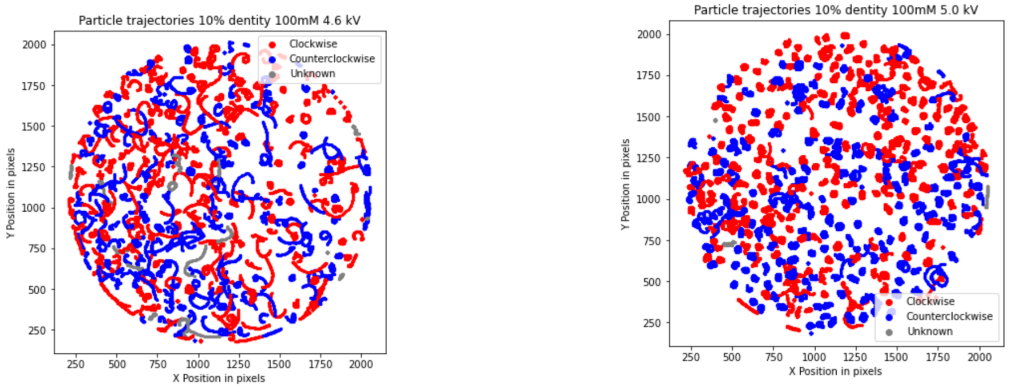

Figure 4.13: *4.6 kV, left: high diffusion coefficient. 5.0 kV, right: low diffusion coefficient. 10% packing density in 100 mM.*

From these measurements, we observe that particles become active more quickly in the 10% packing density system compared to the 40% packing density system as there are more stationary particles in the 40% packing density system at the same voltage. This is because in higher density systems clusters are formed due to the limited available space for individual particle movement. When particles collide with each other or with the walls, they are more likely to become stationary. As a result, in higher density system a higher voltage is required to ensure that all particles are moving.

4.4 Spin-Spin correlation

We are investigating the collective motion of active chiral particles, and in this section we focus on the influence of spin orientation on neighbouring particles in the 10% and 40% packing density systems. Although our measurements showed no significant preference for clockwise or counterclockwise spins, we intent to determine if there are localized spin correlations within the spin field.

For the 100 mM, we typically find a spin correlation like this:

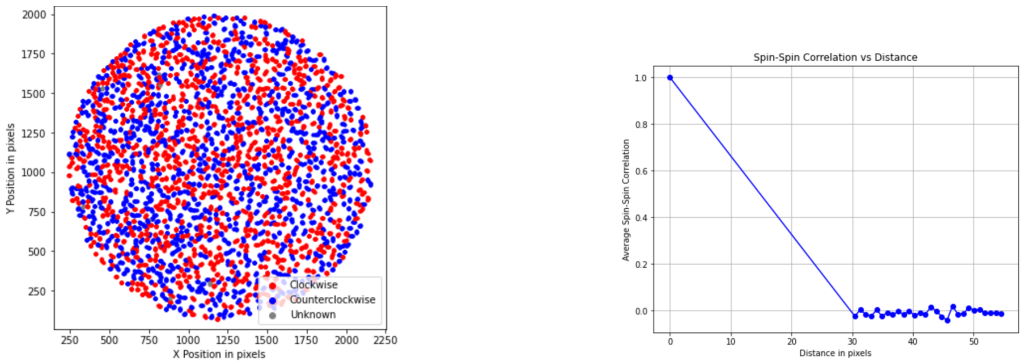

Figure 4.14: *Example of the spin field where red is a clockwise spinning particle and blue is a counterclockwise spinning particle, and the corresponding spin-spin correlation for 40% density, 4.7 kV 100 mM. Distance between two POM beads centers if they touch, is 30 pixels, which is the first measurement point.*

This spin-spin correlation, averaged over space and time, was measured for the 40% packing density system at 4.7 kV. The measured distance is in pixels, with a spin-spin correlation value of 1 at a distance of 0, indicating correlation with itself. The first measurement point is at 30 pixels, corresponding to the distance between the centers to two POM beads

in contact. The spin-spin correlation drops to 0 immediately beyond this point, indicating that there is no consistent or significant influence from the spin orientation of the neighbouring particles on other particles in the 40% packing density system.

However for the 10% packing fraction system at 100 mM system we typically find something more like this:

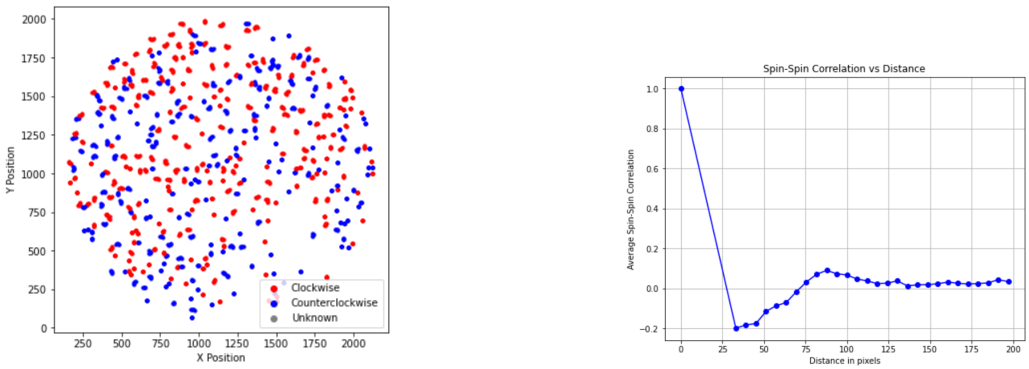

Figure 4.15: *Example of the spin field where red is a clockwise spinning particle and blue is a counterclockwise spinning particle, and the corresponding spin-spin correlation for 10% density, 4.3 kV 100 mM. Distance between two POM beads centers if they touch, is 30 pixels, which is the first measurement point.*

For the 10% packing density system at 100 mM, a negative spin-spin correlation is observed. This phenomenon arises because at this density and concentration particles with opposite spin directions can spin cohesively when they are close together. This results in opposite spinners interaction and exhibiting synchronized motion, moving in the same region.

For lower concentrations, the previously observed negative correlation between spinners is no longer apparent. Only at the 100 mM concentration do we find that individual spinning creates hydrodynamic interactions that dominates over interactions from collisions. At this concentration, the system exhibits more consistent behaviour, characterized by higher angular velocities and steady bouncing. Note that this phenomena does not occur consistently at every voltage for the 100 mM concentration and 10% packing density. Instead it is something that sometimes happens but it is not guaranteed for every measurement withing the right concentration and voltage range.

Chapter 5

Conclusion and discussion

The primary goal of this research was to lay the groundwork for creating a chiral fluid, in which the individual particles are chiral themselves and having the possibility of tuning the parameters in the right conditions, without imposing a spin distribution. We successfully created such particles with the desired dynamics and have investigated the individual and collective dynamics, and found interesting results. For single particles, we observed that they likely exhibit a random spin distribution. The most tuneable parameters for the single particle were found in the 20 mM concentration, which was also the concentration where the transition from non-bouncing to bouncing of the metal bead occurred.

When comparing the dynamics of the multiple particle system and the single particle at the 20 mM concentration, transitions were seen in the angular velocity and the radius of gyration graphs. For the multiple particle system these transitions occurred around 2.40 kV while for the single particle system, this was at 1.90 kV. This shift can not simply be described by the different behaviour for the higher densities, like it was for the other measurements; it was likely due to a concentration error, coming from a previously unknown error in the scale.

When increasing the density of the system at the 20 mM concentration, cluster formation was observed, making it challenging to activate the particles even above the Quincke threshold, especially in the 40% packing density system. From the multiple particle systems, the 40% density system exhibited generally smaller radii of gyration compared to the 10% system due to spatial limitations. While the diffusion coefficient increased with increasing voltages for both densities, the increase was more pronounced in the 10% system, due to more space per particle for movement. Higher concentrations corresponded to higher Quincke thresholds, con-

sistent with theoretical expectations.

At the 100 mM concentration, the 10% packing density system initially increased its diffusion coefficient for increasing voltage, followed by a decrease, which was unexpected. This decrease can be ascribed to the high angular velocity of the particles, exerting hydrodynamic interactions, causing them to spin independently in place and thereby reducing the diffusive behaviour. Another interesting observation at the 100 mM concentration is that the more densely packed system provided clearer dynamical dependencies on voltage than the single-particle dynamics. This highlights that for high densities, particles will take over similar motion as the surrounding particles, as they are influenced to move cohesively.

Interestingly, we hypothesized that the 40% packing density system would likely have pronounced spin-spin correlations due to the close interparticle distances, forcing them to interact. However, our findings demonstrate that only the 10% density system shows a spin-spin correlation that does not immediately decay to 0, even when averaged over space and time. Yet, this correlation is negative, suggesting that particles in 100 mM tend to get opposite spin when they are close together under certain voltages. Particles with opposite spin orientations can spin cohesively when they are close together, resulting in opposite spinning interaction and exhibiting synchronized motion, moving in the same region.

Another promising observation is that the 10% density system at high voltages in the 100mM, there seems to be a separation of spin orientation in space. Although this is not evident from the measurements on the spin-spin correlation, figure 4.13 and other images suggest a distinction between clockwise and counterclockwise spins. This phenomena would be an interesting next step in this study to explore, including its evolution over time. If further studies were to be conducted using the same setup, focusing on the 100 mM concentration would be advisable, as it yields the most intriguing results.

Previous studies on active chiral particles found that at low particle densities, rotational motion exceeds translational motion [14]. Our findings confirms this observation, as the diffusion coefficient, indicative for the translational motion, is also generally higher for the 10% density compared to the single particle. However, at 40% density, the diffusion coefficient is generally lower than for the 10% density. This might be ascribed to the increased interactions between particles at this density, limiting their translational motions.

Another finding from this previous study [14] was that the contact time between like-spinners is generally longer than between opposite spinning particles. This breaks the symmetry compared to otherwise identical par-

ticles, resulting in an attraction between like-neighbouring spinners. From this experiment, we do not see this clearly from the spin-spin correlation data, however there seems to be promising indications of a separation between clockwise and counterclockwise spinners. This observation suggests the potential attraction between like-spinning particles, calling for further investigation.

Other studies [3], [15] noted that chiral fluids are composed of many dynamically or geometrically chiral particles, which can break time-reversal symmetry and mirror symmetry, which often perform impressive collective phenomena, especially chiral flows. However in our research, we did not observe chiral flows, even at the highest densities, this was not found. At 40% density, ensuring all the particles to spin, we require a high concentration and high voltage. Under these conditions, particles have high velocities, frequent collisions and fast changes in trajectory, which do not show any significant spin-spin correlation and prevent the formation of collective chiral flows. At 10% density, chiral flows were also absent, however, we did find promising indications of spin correlations.

In summary, to advance towards further investigating the collective dynamics of an active chiral particle system, we need to optimize the appropriate balance in particle density: excessively high densities should be avoided as that leads to frequent collisions, preventing them from moving together with same spin particles. Next to that, high density is not necessarily beneficial due to the repulsive interactions between the metal beads. Instead, a more balanced density is preferred that allows for hydrodynamic interactions without excessive collisions.

Our study provided valuable insights into the fundamental dynamics of tuneable active chiral particles on the collective level. This research made an advancement in the development of spin-fluids and has opened ways for further exploration. The question of whether a chiral fluid can be achieved with these tuneable particles, remains open. Regardless, future research potentially reveal fascinating new phenomena within the system.

Version of June 14, 2024– Created June 14, 2024 - 14:44

Chapter 6

Appendix

6.1 Quincke electro-rotation

In dielectric particles, charges are naturally bound to specific atoms and are confined to move only within these atoms. When a dielectric particle is exposed to an electric field, the atoms within the particle undergo polarization, creating dipole moments. During this process, the positive nuclei of each atom orients towards the direction of the electric field, while the electrons are pushed in the opposite direction. The attractive forces within the particle and repulsive forces induced by the external electric field reach a balance which leads to the overall polarization of the particle. This dipole moment points in the direction of the induced electric field in the particle, which is anti-parallel to the applied external electric field.

Due to the induced dipole in the particle, which is anti-parallel to the applied electric field, charges from the conductive solvent will distribute themselves on the surface of the particle. Spontaneous symmetry breaking can occur because the dipole moment within the particle tends to align with the applied electric field, which results in a lower potential energy for the system compared to when the dipole moment is not aligned with the field:

$$U = -\vec{p} \cdot \vec{E} \tag{6.1}$$

Where U is the potential energy, $\vec{p}$ is the induced dipole moment in the dielectric particle and $\vec{E}$ is the applied electric field. The induced torque is described by the following equation:

$$\vec{\tau} = \vec{p} \times \vec{E} \tag{6.2}$$

Note that the torque tries to align the dipole moment parallel to the electric field. So when there is a slight instability that can break the symmetry of the configuration at any position, there is a torque that induces rotation of the particle in any direction [5].

This happens above the Quincke threshold, where the induced torque is large enough so we expect to observe rotation of the particle. The rate of rotation of the particle is given by:

$$\omega_Q = \pm \frac{1}{t_{mw}} \sqrt{\frac{E^2}{E_Q^2} - 1} \tag{6.3}$$

where E_Q is the Quincke threshold and E is the applied electric field. The t_{mw} represents the Maxwell-Wagner relaxation time [16]:

$$t_{mw} = \frac{\epsilon_s}{\sigma_s} \left(\frac{\frac{\epsilon_p}{\epsilon_s} + 2}{\frac{\sigma_p}{\sigma_s} + 2} \right) \rightarrow \sigma_p = 0 \rightarrow t_{mw} = \frac{\epsilon_p + 2\epsilon_s}{2\sigma_s} \tag{6.4}$$

So a low conductivity of the solvent (low AOT concentration) would result in a high Maxwell-Wagner relaxation time, and thus a low rate of rotation of the particle.

6.2 Contact charge electrophoresis

In the case of contact charge electrophoresis, when the conductive particle has lifted off of the bottom electrode and is immersed in the conductive solvent, the charge is dissipated on a timescale $\tau_r = \frac{\epsilon_s}{\sigma_s}$. The more ions in the solution (more AOT), the higher the conductivity of the solvent and the lower the timescale to dissipate the charge. The repulsive force on the charge becomes:

$$\vec{F}_e = \frac{2}{3} \pi^3 \epsilon_s \epsilon_0 a^2 E_0^2 e^{-t/\tau_r} \tag{6.5}$$

The other forces working on the conductive bead, are the gravitational force and the hydrodynamic drag force [9]. When the bead reaches the top, it gets the opposite charge, and the electrostatic force has a downward direction, increasing the downward velocity. There are 3 regimes:

1. The conductive bead does not leave the bottom electrode: $\vec{F}_e < \vec{F}_g$.
2. The conductive bead leaves the bottom electrode but does not reach the top. In this case $\vec{F}_e(t_1) > \vec{F}_g$. This happens for example when the

electric field is increased. The conductivity of the solvent plays an important role as well, because the charge dissipates in the solvent. In this case, the charge of the bead is dissipated before the bead had reached to top, so then $\vec{F}_e(t_2) < \vec{F}_g + \vec{F}_d$

3. The conductive bead leaves the bottom electrode: $\vec{F}_e(t_1) > \vec{F}_g$. When the electric field is high enough, the conductive bead could reach the top. The charge did not completely dissipate in the solvent and $\vec{F}_e(t_2) > \vec{F}_g + \vec{F}_d$ so the bead reaches the top electrode and gets the opposite charge. Now the electrostatic force changes direction and accelerates towards the bottom electrode.

6.3 Dynamics of a single spinner

To develop an understanding of the collective dynamics of spinning particles, we investigate a preliminary model in which the particles are approximated to be two-dimensional spinning disks. For this model, we investigate the influences on the dynamics of a single spinner.

The equation of motion that describes a spinning particle i, surrounded by other spinning particles j is formulated as follows:

$$m\ddot{\vec{r}} = \sum_{j \in \delta_i} \vec{F}_{ij} \tag{6.6}$$

$$\vec{F}_{ij} = -\nabla_i U(\vec{r_{ij}}) - \gamma(\vec{r_{ij}})\vec{v}_{ij} + \gamma(\vec{r_{ij}})\vec{w}_{ij} \times \vec{r}_{ij} + \vec{F}_d \tag{6.7}$$

Where in equation 6.6, m is the mass of the particle and $\vec{r}$ is the position vector [13]. $\vec{F_{ij}}$ in equation 6.7 is the pairwise force which contains a conservative part: the gradient of the potential -$\nabla_i U(\vec{r_{ij}})$. In the system for this research the potential would be coming from the electrical interactions as the metal beads are charged.

The second and third term of equation 6.7 represent the non-conservative forces. The term -$\gamma(\vec{r_{ij}})\vec{v}_{ij}$ describes that particles want to move with the same velocity. As the velocity difference $\vec{v_{ij}}$ becomes 0, this term would not contribute to the pairwise forces. $\gamma(\vec{r_{ij}})$ describes a frictional coefficient due to the interactions between particles, depending on the distance between them. The frictional coefficient increases as particles move closer, and with $\gamma(\vec{r_{ij}} \to \infty)$ approaching zero as the particles move apart.

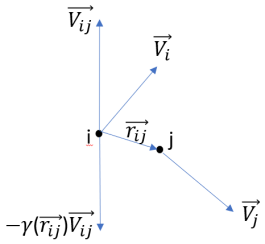

Figure 6.1: *A non-conservative force from the equation of motion of a spinning particle: $-\gamma(\vec{r}_{ij})\vec{v}_{ij}$, causes particle i to be pushed in the same direction as particle j is moving into. $\gamma(\vec{r}_{ij})$ is a frictional coefficient between particle i and j, that depends on the distance between them. $\vec{v}_i$ and $\vec{v}_j$ are the initial velocities of particles i and j velocities, respectively.*

The third term: $\gamma(\vec{r}_{ij})\vec{w}_{ij} \times \vec{r}_{ij}$, describes a force that either pushes rotating particles in the same direction or in the opposite direction, depending on their spin orientation and distance between them. $\vec{w}_{ij}$ is the mean angular velocity of particle i and j. When both particles have the same angular velocity, then the resulting force on i is in the opposite direction as the resulting force on j. If both particles have the same absolute value for the angular velocity but in opposite direction, then the resulting force on i is in the same direction as the resulting force on j.

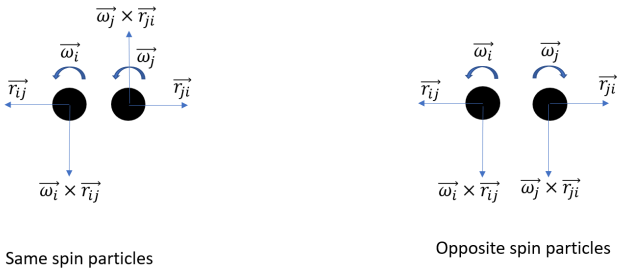

Figure 6.2: *A non-conservative force from the equation of motion of a spinning particle, $\gamma(\vec{r}_{ij})\vec{w}_{ij} \times \vec{r}_{ij}$, is a force that either pushes rotating particles in the same direction or in the opposite direction, depending on their angular velocity and distance between them. $\vec{w}_{ij}$ is the mean angular velocity of particle i and j. $\vec{r}_{ij}$ is the distance between the particles and $\gamma(\vec{r}_{ij})$ is a friction coefficient between particle i and j, that depends on the distance between them.*

The last term $\vec{F}_d$ is a drag term and accounts for the resistance experienced by the particle due to the surrounding solvent. This drag term has the following form:

$$\vec{F}_d = k\eta\vec{v}_i A_i \tag{6.8}$$

where k is a constant, η is the viscosity of the solvent, $\vec{v}_i$ is the velocity of the particle and A_i is the area of the particle.

To complete the model for the dynamics of a spinning particle, we investigate mutual torque between two particles:

$$I\ddot{\alpha} = \gamma_r(\omega_o - \omega_i) + \sum_{j\in\delta_i} \vec{r}_{ij} \times \vec{F}_{ij} \tag{6.9}$$

In equation 6.9, I is the moment of inertia of the particle and α is the angle that the particle makes with itself relative to its initial position so that $\omega = \dot{\alpha}$ is its angular velocity [13].

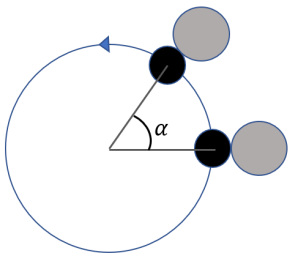

Figure 6.3: *The particle makes an angle α relative to its initial position.*

The first term of the equation, $\gamma_r(\omega_o - \omega_i)$, accounts for the internal and frictional torque which reaches a balance in case of steady state. In this term, γ_r is the rotational friction exerted by the surrounding fluid [17]. ω_0 is the angular velocity of the particle in steady state and ω_i is the actual angular velocity of particle i.

Before the particle reaches steady state: $I\ddot{\alpha}_i \neq 0$ and from that follows that $\omega_o \neq \omega_i$. In this case, the particle tends to accelerate or decelerate towards the steady state angular velocity. When the particle reaches steady state: $I\ddot{\alpha}_i = 0$, so $\omega_o = \omega_i$.

Because we take into account that the particle can spin with both orientations, we consider a Landau potential that describes the free energy potential of our system. This potential has the following form [18]:

$$H(\omega_i) = -\frac{a_2\omega_i^2}{2} + \frac{a_4\omega_i^4}{4} \tag{6.10}$$

In this equation, a_2 and a_4 are constants. If we take the negative derivative of this potential with respect to ω_i, we find the torque of the particle:

$$-\frac{dH(\omega_i)}{d\omega_i} = I\ddot{\alpha} = \omega_i(a_2 - a_4\omega_i^2) \tag{6.11}$$

From here we find the angular velocity of particle i in steady state. We require that $I\ddot{\alpha} = \omega_i(a_2 - a_4\omega_i^2) = 0$. Therefore:

$$\omega_i = \sqrt{\frac{a_2}{a_4}} = \omega_0 \tag{6.12}$$

The second term of equation 6.9, $\sum_{j\in\delta_i} \vec{r}_{ij} \times \vec{F}_{ij}$ accounts for the torque due to interactions, containing the previously mentioned pairwise force $\vec{F}_{ij}$ and the distance vector $\vec{r}_{ij}$, taking into account influences from neighbouring particles. If the pairwise force pushes the particles in the same direction (see image 6.2), the particles' torques have the same sign, and vice versa.

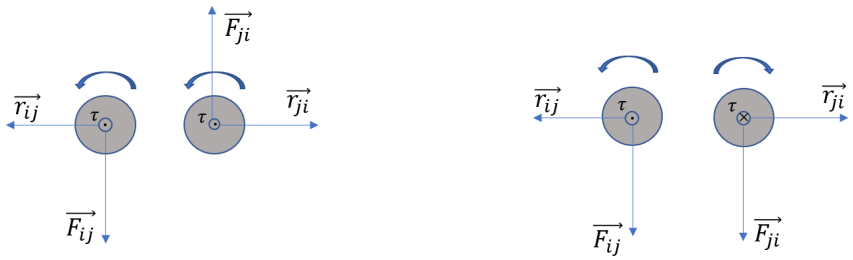

Figure 6.4: *The second term of the equation of mutual torque between two particles, $\sum_{j\in\delta_i} \vec{r}_{ij} \times \vec{F}_{ij}$ describes the torque due to interaction of neighbouring particles. The $\vec{r}_{ij}$ is the distance vector between the two particles and the $\vec{F}_{ij}$ is the pairwise force as described in equation 6.7.*

6.4 Collective motion of spinning particles

During a head-on collision between two spinning particles, the friction between them converts intrinsic angular momentum (due to the spinning on its axis) into orbital angular momentum, creating a circular motion around the center of mass of the two particles. After the collision, the particles move away from each other with a spinning that is reset to the initial angular velocity, but not necessarily with final velocities that are parallel to the vector distance between them. It indicates that the particles have acquired a component of motion perpendicular to their initial trajectory. This means that the orbital angular momentum is generated in the collision [19].

The contact time for like-spinners is generally longer than the contact time for opposite spinners. This breaks the symmetry compared to otherwise identical particles, resulting in an attraction between like-neighbouring spinners.

6.5 Stress and odd viscosity

The evolution of chiral systems in 2 dimensions are mostly governed by the forces in between the neighbouring particles, which is captured by the stress tensor [15]:

$$\sigma_{ij} = C_{ijkl}\delta_l u_k + \eta_{ijkl}\delta_l v_k + ... \tag{6.13}$$

Equation 6.13 describes the surface forces between the particles, in which C_{ijkl} is the elasticity tensor and $\delta_l u_k$ is the displacement gradient. η_{ijkl} is the viscosity tensor and $\delta_l v_k$ is the velocity gradient. The internal forces in the system are then described by:

$$f_i = \delta_j \sigma_{ij} \tag{6.14}$$

In conventional fluids the viscosity tensor η_{ijkl} is a measure of the resistance of the fluid against inhomogeneities in its velocity field, in other words, it describes the irreversible dissipation of energy. The viscosity tensor usually is symmetric under exchange of pair of indices (for time-reversed symmetry). This means that $\eta_{ijkl} = \eta_{klij}$.

However, if the viscosity is not symmetric then $\eta_{ijkl} \neq \eta_{klij}$, which is called odd. More precisely; it flips sign when the pairs of indices are exchanged: $\eta_{ijkl} = -\eta_{klij}$.

6.5.1 Origin of odd viscosity

When there are velocity gradients present in a system, forces appear between the neighbouring particles, that tend to make the velocities equal. The stress tensor captures those forces. If we rewrite equation 6.13, we get:

$$\sigma_{ij} = \sigma_{ij}^h + \sigma_{ij}^{vis} \tag{6.15}$$

Where σ_{ij}^h describes the hydrostatic stresses that are present in usual fluids at rest and $\sigma_{ij}^{vis} = \eta_{ijkl}\delta_l v_k$ describes the viscous stresses induced by the velocity gradients. The viscous force density is given by $f_i^{vis} = \delta_j \eta_{ijkl}\delta_l v_k$, according to equation 6.14.

When the rate of mechanical energy loss by viscous dissipation per unit volume is investigated, it appears that only the symmetric part of the viscosity tensor contributes to the dissipation [15]:

$$\dot{\omega} = \sigma_{ij}^{vis}\delta_j v_i = \eta_{ijkl}^{s}(\delta_j v_i)(\delta_l v_k) \tag{6.16}$$

Where $\eta_{ijkl}^{s} = \frac{[\eta_{ijkl}+\eta_{klij}]}{2}$ is the symmetric part of the viscosity tensor, the only part that contributes to energy dissipation. The antisymmetric part $\eta_{ijkl}^{a} = \frac{[\eta_{ijkl}-\eta_{klij}]}{2}$ that describes the nondissipative viscosity, drops out. This is what we call the odd viscosity. This odd viscosity does not lead to energy dissipation like in conventional fluids, but rather ensures that a fluid flows perpendicular to the applied pressure. [19].

In chiral fluids, the spinning particles are driven by active forces. That causes the stress tensor to be anti-symmetric $\sigma_{ij}^{a} = \frac{(\sigma_{ij}-\sigma_{ji})}{2}$ and corresponds to a torque $\tau_i = \frac{1}{2}\epsilon_{ijk}\sigma_{jk}^{a}$. Odd viscosity contributes to this anti-symmetric stress. This complex stress tensor leads to unusual behaviour in the materials response to stress. This anti-symmetric stress is an important factor in causing a chiral flow [19], which in turn can allow for the emergence of hyperuniform structures [3] and collective phenomena [14].

6.5.2 Evolution of the chiral flow due to pressure difference

Odd viscosity can have effects on how a fluid flows and can change the solutions of the Navier-Stokes equations. If we look at incompressible 2d flow and only consider shear viscosities, the Navier-Stokes equation is as follows [15]:

$$\rho D_t \vec{V} = -\nabla P + \eta\Delta\vec{V} + \eta^0\vec{\epsilon}\cdot\Delta\vec{V} \tag{6.17}$$

with $\nabla\cdot\vec{V} = 0$ because we assume an incompressible flow. The odd viscosity η^0 induces a viscous force perpendicular to the expected force from shear viscosity. Consider a poiseuille flow in 2 dimensions without odd viscosity.

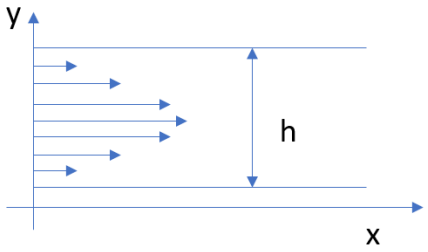

Figure 6.5: *Usual 2D poiseuille flow velocity profile.*

Such a conventional fluid that experiences 2D Poiseuille flow through a channel with constant pressure gradient $G = \frac{dP}{dx}$, the velocity field is of the following forms:

$$\vec{V} = \frac{G}{2\eta} y(h-y)\hat{e}_x \tag{6.18}$$

If we now switch to a system with odd viscosity η^0 and if the boundary conditions only involve the velocity of the fluid, the velocity field of a 2D fluid with and without η^0 are indistinguishable, in other words, $\vec{V} = \vec{V}'$, where $\vec{V}'$ denotes the velocity field of a fluid with an odd viscosity.

Let's take a closer look at $\vec{\epsilon} \cdot \Delta\vec{V}$. First of all the Laplacian of the velocity vector is a constant in direction:

$$\Delta\vec{V} = \frac{\delta^2}{\delta y^2}\left(\frac{G}{2\eta} y(h-y)\hat{e}_x\right) = -\frac{G}{\eta}\hat{e}_x \tag{6.19}$$

The levi-Civita symbol is defined as follows: $\vec{\epsilon} = \begin{pmatrix} 0 & 1 \\ -1 & 0 \end{pmatrix}$.

$$\vec{\epsilon} \cdot \Delta\vec{V} = \frac{G}{\eta}\hat{e}_y \tag{6.20}$$

So the velocity field is the same, but simply rotated clockwise by 90°. We can use the identity $\vec{\epsilon} \cdot \Delta\vec{V} = \nabla\omega$.

Now if we introduce the effective pressure:

$$P' = P - \eta^0\omega \tag{6.21}$$

Where P' is the pressure in the system with odd viscosity. We note that $P' = P$ for a system without odd viscosity. Then we could rewrite the Navier-Stokes equation as follows:

$$\rho D_t \vec{V}' = -\nabla P' + \eta\Delta\vec{V}' \tag{6.22}$$

Now if we remember the $\omega = \epsilon_{kl}\delta_k V_l = \delta_x V_y - \delta_y V_x$, which we can solve by taking the derivative of V_x with respect to y ($\vec{V}$ only has a x-component), we get:

$$\omega = -\frac{G}{2\eta}(h - 2y) \tag{6.23}$$

Now $P = P' + \eta^0\omega = P' - \frac{G\eta^0}{2\eta}(h - 2y)$. This term is normally top-down symmetric if we have a flow without odd viscosity. The pressure difference measured between the top and the bottom of the channel in an odd viscous fluid is:

$$\Delta P = P(h) - P(0) = Gh\frac{\eta^0}{\eta} \tag{6.24}$$

This pressure difference compensates for the fact that the particles are building up on the edges of the confinement.

6.6 Relevant Constants and calculations

6.6.1 Constants and physical properties

Quantity	Symbol	Value
Radius of the metal bead	a	5×10^{-4} m
Density of the stainless steel bead	ρ_p	7800 kg/m^3
Density of hexadecane	ρ_s	773 kg/m^3
Gravitational acceleration on Earth	g	9.81 m/s^2
Dielectric constant of hexadecane	ϵ_s	2.04 ϵ_0
Vacuum permittivity	ϵ_0	8.85×10^{-12} F/m

Table 6.1: *Constants and physical properties used in calculations.*

6.6.2 Calculations for packing densities

Particle radii and area calculations

- Radius of POM bead: $r_1 = 0.794$ mm
- Radius of metal bead: $r_2 = 0.5$ mm

- Combined area of one particle (top view):

$$\text{Area}_p = \pi r_1^2 + \pi r_2^2 = \pi(0.794^2 + 0.5^2) \approx 2.77\,\text{mm}^2 \tag{6.25}$$

Circular confinement area

- Radius of outer circular confinement: $r_3 = 60$ mm
- Area of circular confinement:

$$\text{Area}_c = \pi r_3^2 = \pi \times (60)^2 \approx 11310\,\text{mm}^2 \tag{6.26}$$

Number of particles for packing densities

- **10% Packing density**:

$$\text{Number of particles} = \frac{0.1 \times \text{Area}_c}{\text{Area}_p} = \frac{0.1 \times 11310}{2.77} \approx 408\,\text{particles} \tag{6.27}$$

- **40% Packing density**:

$$\text{Number of particles} = \frac{0.4 \times \text{Area}_c}{\text{Area}_p} = \frac{0.4 \times 11310}{2.77} \approx 1633\,\text{particles} \tag{6.28}$$

Packing density	Total area occupied (mm^2)	Area per particle (mm^2)	Number of particles
10%	1131	2.77	408
40%	4524	2.77	1633

Table 6.2: *Number of particles required for different packing densities.*

6.7 60 mM measurements

6.7.1 Radius of gyration & angular velocity

The results for the radius of gyration and angular velocity as a dependency on voltage for 10% and 40% packing density for the 60 mM concentration are presented:

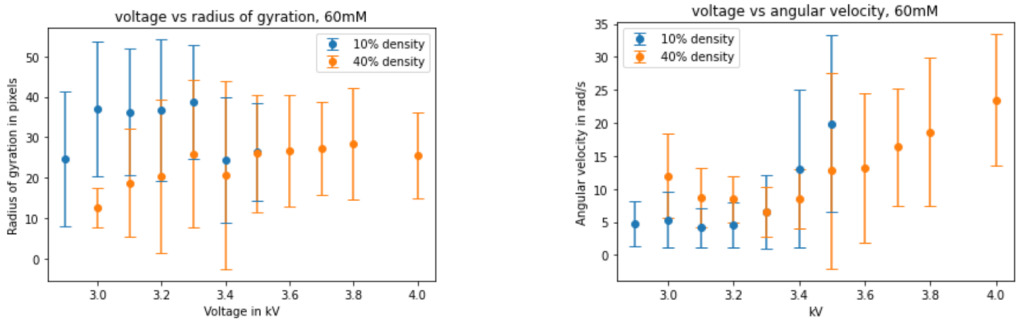

Figure 6.6: *Radius of gyration and angular velocity for the 10% and 40% packing density systems at 60 mM.*

From the lowest measured voltages onwards we are already in the regime where the metal bead bounces. Still we see that only after approximately 3.3 kV, there is an increase in angular velocity and a plateau (40%) or decrease (10%) in the radius of gyration. This is also seen in the single particle measurements for this concentration.

For the single spinner, we observed radii of gyration between 27 and 39 pixels. For the 10% packing density this is between, 24 and 38 pixels which is a similar regime but for the 40% packing density the observed radii of gyration is between 12 and 29 pixels, which is significantly lower, like in the 20 mM concentration. For both the 10% and 40% packing density, the range of angular velocity is significantly lower than for the single particle.

6.7.2 Cluster formation & diffusion coefficient

The results for the percentage of stationary particles and diffusion coefficient for the 10% and 40% packing densities for the 60 mM concentration are shown in figure 6.7:

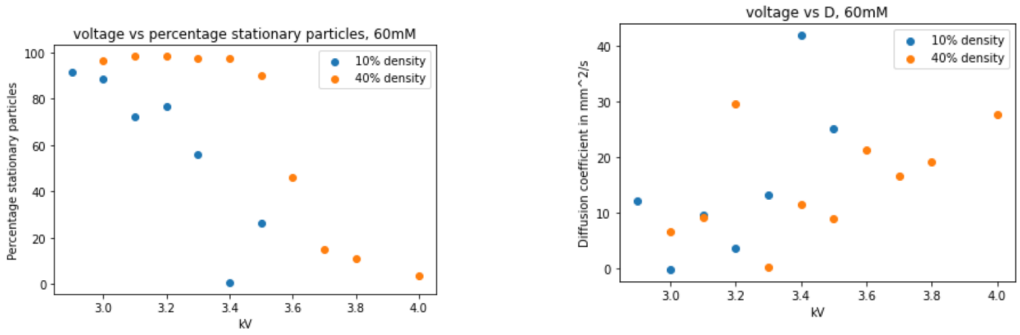

Figure 6.7: *Percentage of stationary particles and diffusion coefficient against applied voltage for 10% and 40% packing density in 60 mM.*

For the 60 mM measurements, we observe a transition from a high percentage of stationary particles for low voltages to a low percentage of stationary particles for higher voltages. However, we cannot draw a significant conclusion about the system's diffusive properties. In this concentration, not all particles have a similar radius of gyration and angular velocity, and therefore the variance is relatively high, leading to unclear correlations. To illustrate, an example image of the trajectories of particles in 60 mM are presented:

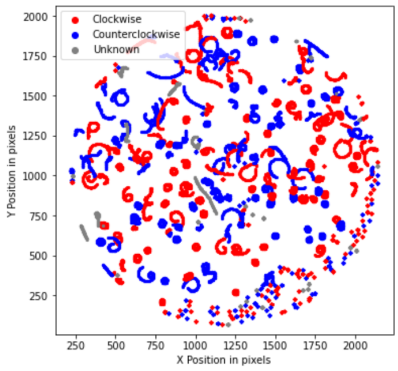

Figure 6.8: *60 mM 10% packing density at 3.5 kV showing different types of behaviour in the system: particles spinning on the spot, particles making larger radii of gyration and stationary particles.*

Nevertheless, the diffusion coefficients are between 0 and 40 mm^2/s, while for the 20 mM measurements they are between 0 and 18 mm^2/s. This increase might be due to the metal bead bouncing consistently, and POM having a higher angular velocity with increasing voltage. Consequently, the metal bead becomes less effective as an anchor, leading to

more diffusion after collisions.

The diffusive behaviour for the denser systems differ from the behaviour of a single spinner, which has a low constant diffusion coefficient for low voltage and increases suddenly for high voltages. This is because the single spinner can not collide with other particles, and the single spinner exerts only one type of behaviour in the system.

Version of June 14, 2024– Created June 14, 2024 - 14:44

Bibliography

[1] B. Liebchen and D. Levis, *Collective Behavior of Chiral Active Matter: Pattern Formation and Enhanced Flocking*, Physical Review Letters **119** (2017).

[2] *Chiral Molecules*, 2015, [Online; accessed 2024-02-28].

[3] M. A. López-Castaño, A. Márquez Seco, A. Márquez Seco, A. Rodríguez-Rivas, and F. V. Reyes, *Chirality transitions in a system of active flat spinners*, Phys. Rev. Res. **4**, 033230 (2022).

[4] M. Ã. LÃ^3*pez* − *CastaÃ* ± *o*, *A*. *Seco*, *A*. *Seco*, *Ã*. *RodrÃguez* − *Rivas*, *and F*. *Reyes*, *Chiralitytransitionsinasystemofactiveflatspinners*, *PhysicalReviewResearc*

[5] G. Fuhr and R. Hagedorn, *The physical principle of Quincke-rotation as a possible explanation for low frequency cellular oscillators*, Journal of Electroanalytical Chemistry and Interfacial Electrochemistry **276**, 1 (1989).

[6] G. E. Pradillo, H. Karani, and P. M. Vlahovska, *Quincke rotor dynamics in confinement: rolling and hovering*, Soft Matter **15**, 6564 (2019).

[7] A. M. Drews, C. A. Cartier, and K. J. M. Bishop, *Contact Charge Electrophoresis: Experiment and Theory*, Langmuir **31**, 3808 (2015), PMID: 25785396.

[8] A. M. Drews, C. A. Cartier, and K. J. M. Bishop, *Contact Charge Electrophoresis: Experiment and Theory*, Langmuir **31**, 3808 (2015), PMID: 25785396.

[9] K. J. M. Bishop, A. M. Drews, C. A. Cartier, S. Pandey, and Y. Dou, *Contact Charge Electrophoresis: Fundamentals and Microfluidic Applications*, Langmuir **34**, 6315 (2018), PMID: 29350535.

[10] J. Schmidt, R. Prignitz, D. Peschka, A. MÃŒnch, B. Wagner, E. BÃ€nsch, and W. Peukert, *Conductivity in nonpolar media: Experimental and numerical studies on sodium AOTâhexadecane, lecithinâhexadecane and aluminum(III)-3,5-diisopropyl salicylateâhexadecane systems*, Journal of Colloid and Interface Science **386**, 240 (2012).

[11] Z. Zhang, H. Yuan, Y. Dou, M. Cruz, and K. Bishop, *Quincke oscillations of colloids at planar electrodes*, 2021.

[12] C. Bacher, M. Reichenzeller, C. Athale, H. Herrmann, and R. Eils, *4-D single particle tracking of synthetic and proteinaceous microspheres reveals preferential movement of nuclear particles along chromatin - Poor tracks*, BMC cell biology **5**, 45 (2004).

[13] B. Liebchen and D. Levis, *Chiral active matter*, Europhysics Letters **139**, 67001 (2022).

[14] N. H. P. Nguyen, D. Klotsa, M. Engel, and S. C. Glotzer, *Emergent Collective Phenomena in a Mixture of Hard Shapes through Active Rotation*, Phys. Rev. Lett. **112**, 075701 (2014).

[15] M. Fruchart, C. Scheibner, and V. Vitelli, *Odd Viscosity and Odd Elasticity*, Annual Review of Condensed Matter Physics **14**, 471â510 (2023).

[16] M. Iwamoto, *Maxwell–Wagner Effect*, pages 1276–1285, Springer Netherlands, Dordrecht, 2012.

[17] P. Nelson and M. RadosavljevicÌ, *Biological physics : energy, information, life*, Freeman, New York, NY [etc, 1st print. edition, 2004.

[18] C. Nigro, *Phase field modeling of flaw-induced hydride precipitation kinetics in metals*, PhD thesis, 2017.

[19] D. Banerjee, A. Souslov, A. G. Abanov, and V. Vitelli, *Odd viscosity in chiral active fluids*, Nature Communications **8**, 1573 (2017).